

DEFORMATION HISTORY OF ULTRA HIGH-PRESSURE OPHIOLITIC SERPENTINITES IN THE ZERMATT-SAAS ZONE, CRÉTON, UPPER VALTOURNANCHE (AOSTA VALLEY, WESTERN ALPS)

Pietro Luoni^{*✉}, Davide Zanoni^{*}, Gisella Rebay^{**} and Maria Iole Spalla^{*}

^{*} Dipartimento di Scienze della Terra “A. Desio”, Università degli Studi di Milano, Italy.

^{**} Dipartimento di Scienze della Terra e dell’Ambiente, Università degli Studi di Pavia, Italy.

✉ Corresponding author, e-mail: pietro.luoni@unimi.it

Keywords: *serpentinites; foliation trajectory map; multi-scale structural analysis; Ti-chondrodite; Ti-clinohumite; subduction tectonics; Western Alps.*

ABSTRACT

Detailed multiscale structural analyses and mapping (1:20 scale) integrated with petrological investigation were used to study a portion of the Zermatt-Saas serpentinites that crop out in upper Valtournanche (north-western Italy). Results are synthesized in a foliation trajectory map that displays the transposed original lithostratigraphy of a serpentinite body exposed at Créton. The serpentinite body comprises magnetite sheets and rare, decimetre-thick, diopside layers and lenses. Moreover, veins and aggregates of Ti-chondrodite and Ti-clinohumite, olivine-rich layers and lenses, veinlets of olivine, and layers of dark pyroxenite are embedded in the serpentinites. Serpentinites and associated rocks record three relative age groups of ductile structures: D₁ consists of rare folds and S₁ foliation; D₂ is a group of isoclinal folds and a very pervasive foliation (S₂), which is the dominant structure; D₃ includes a crenulation and shear zones affecting S₂. The detailed meso-structural and microstructural analyses allowed individuating the metamorphic environment of successive deformation stages and correlating the resulting tectono-metamorphic investigation with those already inferred in surrounding areas. In addition, metre- to submillimetre-sized pre-D₂ structural, mineralogical, and textural relics have been clearly identified in spite of the strong transposition imposed during the development of S₂ high pressure - ultra-high pressure foliation.

INTRODUCTION

Serpentinites are ever more considered as key players in processes that involve lithosphere subduction and exhumation. Their structural and metamorphic evolutions are poorly explored with respect to those of crustal rocks due to their extreme plasticity and generally high compositional homogeneity (e.g. Scambelluri et al., 1995; Li et al., 2004; Grigull et al., 2012; Rebay et al., 2012a; 2012b). Because of their low viscosity, the structural overprinting relationships in Alpine serpentinites are often very rich and therefore well-exposed key-outcrops preserving a long tectonic record, such as primary lithological heterogeneities, deserve extreme analytical care. In localities close to Créton, detailed petrostructural analysis (Zanoni et al., 2012; 2016) reconstruct the deformation history of serpentinites and rodingites and allow recognizing primary and metamorphic relic assemblages, often just preserved as single porphyroclasts. Generally during field mapping in the axial portion of orogenic belts, lithostratigraphic, structural and petrological observations are integrated into a modern structural map that reports foliation trajectories over the finite lithostratigraphic framework (Gosso et al., 1983; Passchier, 1990; Johnson and Duncan, 1992; Connors and Lister, 1995; Zucali et al., 2002; Gosso and Spalla, 2009; Baletti et al., 2012; Zanoni et al., 2012). The goal is therefore to collect the full assemblage of details on relative structural chronology, textural types reflecting fabric gradients (Gosso et al., 2010; 2015), and mineral assemblages marking successive foliations. The representation techniques can reveal the sequence of superposed textural and metamorphic imprints and allow following the lateral continuity of information that is the key for evaluating the significance of structural and mineral relics distribution at the regional scale. The integrated interpretation of structural

and petrologic data is basic for the reconstruction of the tectonic evolution (e.g. Spalla et al., 2005) and therefore this type of maps permits the recognition of geodynamic settings in which mantle and crust portions of orogenic scars have been forged during mountain building processes.

This approach is here applied to enclose the structures and lithologies within the tectonic framework of the Zermatt-Saas serpentinites in the upper Valtournanche and to separate the Alpine structures and fabrics from pre-Alpine oceanic relics. Finally, mineral assemblages associated with successive foliations are used to constrain the P-T-d-t evolution of the Créton serpentinites adding a new tile to the Zermatt-Saas Zone (ZSZ) tectono-metamorphic puzzle (Luoni et al., 2018).

GEOLOGICAL SETTING

The ZSZ is part of the Piemonte Zone, in the Penninic domain of Western Alps (Fig. 1a, b) (Bigi et al., 1990; Dal Piaz, 1992; Martin et al., 1994 and reference therein), comprising carbonatic and terrigenous metasediments, minor quartzites, metabasites, metagabbros, eclogites, rodingites, serpentinites, and minor opicalcites. ZSZ is interpreted as a wreckage of the Alpine Tethys that is constituted by an ophiolitic suite typical of a slow-spreading setting (Boudier and Nicolas, 1985; Nicolas and Boudier, 2003) buried at mantle-depths, transposed during Alpine subduction-collision, and at present marking the oceanic scar in the axial zone of Western Alps. ZSZ includes serpentinitized peridotites (Li et al., 2004; Rebay et al., 2012a; 2012b), metagabbros and metarodingites (Li et al., 2004; Rebay et al., 2012a; 2012b; Zanoni et al., 2016), N-MORB metabasites (Bucher et al., 2005 and reference therein), and minor metasediments as calcschists and quartzites (Beauregard, 1967; Ernst and

Dal Piaz, 1978; Tartarotti et al., 2017). The serpentinisation of ZSZ ultramafites was interpreted as mainly due to ocean floor metasomatism responsible also for the rodingitisation of the associated gabbroic dykes (Li et al., 2004; Rebay et al., 2012a; 2012b; Zanoni et al., 2012; Zanoni et al., 2016). The ophiolitic complex locally hosts continental rock slices (Dal Piaz et al., 1983; Kienast, 1983; Weber and Bucher, 2015). The ZSZ rocks are widely deformed under eclogite-facies conditions and successively re-equilibrated

under blueschist- to greenschist-facies conditions (Bearth, 1967; Ernst and Dal Piaz, 1978; Cartwright and Barnicoat, 2002). ZSZ rocks are tectonically coupled and sandwiched with those of the Combin Zone (CZ) between the Monte Rosa and Dent Blanche nappes (Fig. 1b) (Dal Piaz, 1988; Polino et al., 1990; Zingg et al., 1990). The Pancherot-Cime Bianche Unit (PCB) discontinuously marks the boundary between ZSZ and CZ. CZ has been interpreted as derived from an ocean-continent transition zone and is affected by

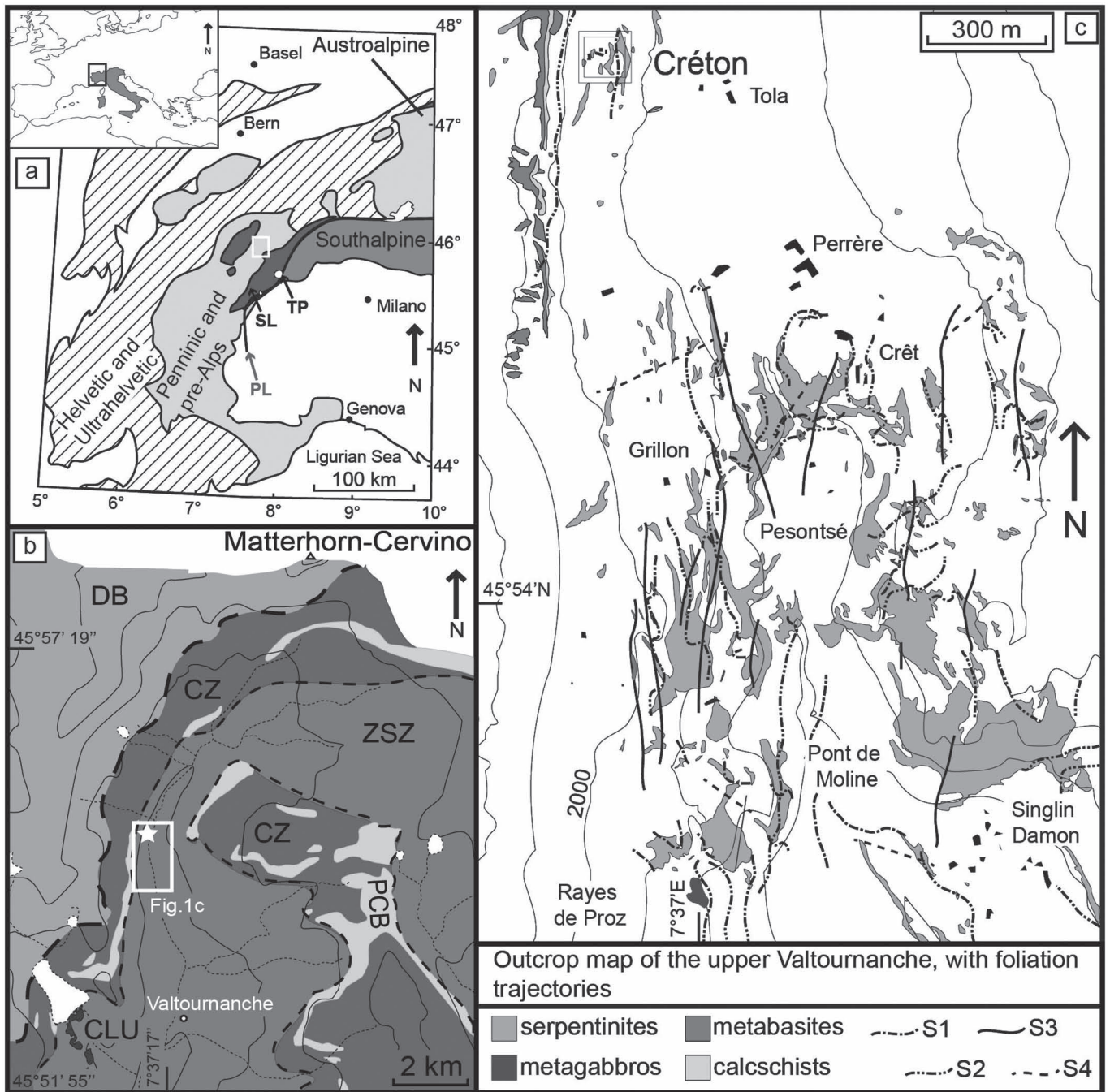


Fig. 1 - a) Simplified tectonic sketch of the Western Alps with the location of the studied area (in the white square). TP- Tertiary plutons; PL- Periadriatic Line; SL- Sesia-Lanzo Zone. b) interpretative tectonic map of the upper Valtournanche (modified after De Giusti et al., 2003). The white star localises Crétón, the white rectangle circumscribes Fig. 1c. ZSZ- Zermatt-Saas Zone; CLU- Cignana Lake Unit (redrawn after Forster et al., 2004); PCB- Pancherot-Cime Bianche Unit; CZ- Combin Zone; DB- Dent Blanche nappe; c) outcrop structural map, modified after Rebay et al. (2018) and by Zanoni (unpublished: original mapping at 1:5000 scale) with the foliation trajectories in the meta-ophiolites of the upper Valtournanche (ZSZ). The double square localises Crétón outcrops. Relative chronology of successive foliation trajectories and rock types are specified in the legend. Topography redrawn from the technical map of the Val d’Aosta Regional Administration, without hydrography.

STRUCTURAL MAP

a dominant metamorphic imprint under greenschist-facies conditions, with poorly preserved blueschist facies relics (Dal Piaz, 1974; Dal Piaz and Ernst, 1978; Ring, 1995; Cartwright and Barnicoat, 2002). PCB has been described as a continental affinity unit and consists of Permian to Cretaceous sedimentary protoliths (Dal Piaz, 1988; 1999). The tectonic contact between ZSZ and CZ has been repeatedly reworked during the Alpine convergence (Ballèvre and Merle, 1993; Pleuger et al., 2007). Radiometric data assign an age to ZSZ protoliths of oceanic metagabbros and metabasites between 164 and 153 Ma in the Swiss portion (Rubatto et al., 1998) and MORB percolations in serpentinites between 168 and 162 Ma in the Italian upper Valtournanche (Rebay et al., 2018).

High pressure - ultra-high pressure peak conditions have been inferred in different localities of the ZSZ. Metabasites of Saas-Fee experienced peak conditions spanning from 1.9-2.2 GPa and 530-600 °C (Dale et al., 2009) and 2.3-2.5 GPa and 530-555 °C (Angiboust et al., 2009) to 2.5-3.0 GPa and 550-600 °C (Bucher et al., 2005). Metagabbros in the ZSZ Swiss portion registered peak conditions at 1.75-2.0 GPa and 550-600 °C (Barnicoat and Fry, 1986), 2.5 GPa and 650 °C (Meyer, 1983) and 2.5 GPa and 610 °C (Bucher and Grapes, 2009). Reinecke (1991) deduced an ultra-high pressure peak of 3.0 GPa and 550-600 °C for quartzites at Lago di Cignana (Cignana Lake Unit = CLU). More recent estimates in CLU indicated conditions from 2.7 to over 3.2 GPa for temperatures between 590 and 630 °C (van der Klauw et al., 1997; Reinecke, 1998; Groppo et al., 2009) and microdiamonds have been discovered in CLU oceanic meta-sediments (Frezzotti et al., 2011) shifting the peak-conditions at $P \geq 3.2$ GPa and $T = 600$ °C. High pressure at the limit with ultra-high pressure peak conditions are also reported in few studies on serpentinites in the Swiss portion of ZSZ, up to 2.0-2.5 GPa and 600-650 °C (Li et al., 2004), and in Valtournanche, where serpentinites experienced 2.2-2.8 GPa and 580-620 °C (Rebay et al., 2012a; 2012b) similarly to the associated rodingites that re-equilibrated at 2.3-2.8 GPa and 580-660 °C (Zanoni et al., 2016). Peak conditions of 2.2-2.3 GPa and 515-645 °C were estimated in a continental slice tectonically embedded in ZSZ ophiolitic rocks at Trockener Steg, in the upper Zermatt valley (Weber and Bucher 2015). In the Créton serpentinites (upper Valtournanche) mapped in this study, Ti-chondrodite relic assemblages allowed to infer 2.8-3.5 GPa and 600-670 °C, indicating that ultra-high pressure assemblages are definitely recorded also in serpentinites (Luoni et al., 2018). Although these Ti-humites bearing assemblages indicate UHP conditions, according to isotopic compositions Gilio et al. (2019) infer a gabbroic origin for their protolith, which was successively metasomatized and recrystallized during subduction.

High pressure peak in ZSZ was dated between 70 and 38 Ma, but ages for prograde metamorphic imprints are assessed at least at 80 Ma (Bowtell et al., 1994; Rubatto et al., 1998; Dal Piaz et al., 2001; Skora et al., 2009; 2015; Springer et al., 2009; de Meyer et al., 2014; Weber et al., 2015; Rebay et al., 2018). Syn- D_2 mineral associations in serpentinites from upper Valtournanche post-date the ultra-high pressure humite-bearing assemblage and have been dated at 65.5 ± 5.6 Ma (Rebay et al., 2018). This wide range of ages and metamorphic conditions is consistent with a heterogeneous tectonic evolution of different portions of the ZSZ meta-ophiolites that recorded diachronic pressure peaks under different P-T conditions.

Heterogeneously deformed metamorphic terrains can provide high quality material for laboratory studies after field structural analyses that infer the chronological sequence of structural and metamorphic imprints (e.g. Hobbs et al., 1976; Passchier, 1990; Spalla and Zucali, 2004; Gosso et al., 2015). Indeed, the studied rocks consist of serpentinites that enclose diopsidite and olivine-rich layers and lenses, issued from thoroughly evolved rheological environments. Our structural map reports the grid of superposed foliations and the related transposition of the lithostratigraphy in adjacent outcrops, integrating also the micro-scale results in the definition of grain-scale layering. To show the reworking of lithostratigraphy in detail, a mapping scale of 1:20 was chosen. The recognition of relic structures and textures and the identification of the oceanic lithostratigraphy was possible despite the strong transposition imposed during the pervasive mylonitization. In the map plate a synthetic scheme (1:200 scale) is reported to locate the outcrops mapped at 1:20 scale. This map was drawn using aerial photos from the Geo-Portal of Valle d'Aosta regional administration (<http://geoportale.partout.it/>). The legend reports lithotypes and fabric elements. Structural orientation data are shown in equal area Schmidt projections (lower hemisphere) separated according to relative chronology. Detailed outcrop maps are georeferenced and the related data are stored into a geodatabase set within a Geographic Information System (GIS) platform. Interpreted 1 m-spaced contour lines have been added on the detailed maps to show the intersection of structures and topography and render the three-dimensional polydeformed lithostratigraphy.

LITHOSTRATIGRAPHY

In upper Valtournanche, serpentinites are dominant and host hectometre-sized metagabbro bodies and metre-sized rodingite dykes and boudins; a pervasive S_2 foliation dominates in serpentinites (Rebay et al., 2012a; 2012b; 2018). Créton alpages are located on a ledge over the western slope of Valtournanche. Here outcrops show whaleback surfaces, which, after a patient iron brushing of mosses and lichens, display a great wealth of structures. Créton serpentinites are located in the structurally uppermost part of ZSZ, close to the tectonic contact with the overlying CZ calcschists and metabasites (Fig. 1c). Two types of serpentinites were distinguished on the basis of textural and mineral features: white porphyroclasts serpentinites and olivine-rich serpentinites. Both serpentinite types contain Ti-chondrodite + Ti-clinohumite veins and olivine. Furthermore, all the serpentinites enclose olivine-rich layers, diopsidites, and pyroxenites. Primary relationships between different rocks are synthesized in Table 1 (row "lithostratigraphy"). Modal amounts were quantitatively evaluated using optical microscope.

The *white porphyroclasts serpentinites* (Fig. 2a, b; outcrop 1 and 2, on the map plate) consist of antigorite (60-90%), magnetite (10-15%), olivine/clinopyroxene (5-10%), calcite + dolomite (< 5%), and locally Ti-clinohumite, chlorite and apatite (< 5%). Generally, an altered surface with white and pale grey oval (up to) centimetre domains in an aqua-green matrix, characterizes this very fine- to fine-grained rock, which is affected by a pervasive mylonitic foliation.

Table 1 - Schematic representation of meso-structures detected in serpentinites and associated rocks.

	Schematic representation of mesostructures	Mesostructural type & style
lithostratigraphy		<p>Lithostratigraphy deformed during Alpine evolution:</p> <ul style="list-style-type: none"> - all the lithotypes are embedded in serpentinite - magnetite layers are crosscut by olivine-rich layers, diopside layers and Ti-chondrodite+Ti-clinohumite veins - olivine-rich layers and lenses are crosscut by Ti-chondrodite+Ti-clinohumite veins
pre-D2		<p>D1 folds: locally olivine-rich layers, magnetite layers and Ti-chondrodite + Ti-clinohumite veins mark hinges of very close folds which are refolded by D2.</p> <p>Pre-D2 foliations:</p> <ul style="list-style-type: none"> - S1 and S₂ in D2 fold hinges. - S1 at high angle with S2, found in a single olivine-rich lens mantled by S2.
D2		<p>S2: Very pervasive mylonitic, locally composite foliation, 14-65/W-WNW dipping, that transposes and mantles the previous structures. S2 occurring at Creton corresponds to the S2 axial plane foliation of D2 folds described by Rebay et al. (2012). The cleavage is associated with boudinage of olivine-rich layers and pyroxenites layers, and olivine and Ti-Chu + Ti-Chn veins.</p> <p>D2 folds: close decimeter-sized folds evidenced by olivine-rich layers and magnetite layers. Magnetite layers are asymmetrically crenulated by D2.</p>
D3		<p>D3 folds: centimeter-sized open folds affecting S2 cleavage. Axial planes and axes are respectively 50-53/307-323 and 1-28/222-246 dipping.</p> <p>D3 shear zones: 5-50 centimeter-long shear zones intersecting S2 cleavage. Shear planes are 32-45/230-246 dipping. The shear sense is sinistral.</p>

The structural setting of rock assemblages in each field reflects the present-day arrangement, whereas bold traces indicate structures related to the described stage (pre-D₂, D₂, D₃).

Olivine-rich serpentinites (Fig. 2c, d; outcrop 1, on the map plate) appear as ochre, yellow to brownish rocks at the altered surfaces. They contain fine-grained antigorite (50-80%), olivine (20-30%), magnetite (5-15%), chlorite (< 5%), and are rich in millimetre- to submillimetre-thick olivine veins. Also in the olivine veins a mylonitic foliation is the dominant fabric (Fig. 2d).

Both serpentinite types are rich in *magnetite layers* (Fig. 2a, c; outcrop 1, on the map plate) constituted by magnetite (50-90%), antigorite (10-30%), and locally olivine (10-20%). Layer boundaries are fuzzy due to the transposition produced during the development of the dominant S₂ foliation. The metre to decimetre alternation of these two serpentinite types, streaked by magnetite layers, could represent an original compositional layering, transposed during Alpine tectonics.

Fine- to coarse-grained *Ti-Chondrodite + Ti-Clinohumite veins*, with Ti-chondrodite + Ti-clinohumite reddish in colour (Fig. 2b, d, e; outcrop 2, on the map plate), occur in almost all the mapped outcrops and are often rimmed by a centimetre whitish antigorite aggregate. They are composed by Ti-chondrodite + Ti-clinohumite (70-80%), olivine (10-20%), antigorite (5-10%), magnetite ± ilmenite (5-10%), chlorite (< 5%).

Diopsidites (Fig. 3a, b; outcrop 1 and 6, on the map plate) are constituted by diopside (whitish crystals) (70-80%), antigorite ± chlorite (10-20%), tremolite + actinolite (5-20%), ilmenite ± titanite (5%) and locally contain magnetite, calcite, and apatite (< 5%). They are fine- to coarse-grained and form grey and ochre layers to lenses parallelized into the dominant foliation. Diopsidites preserve more than one mineral-scale foliation, their boundaries with serpentinites are sharp, and often are rimmed by chlorite schists.

Chlorite schists, constituting 1 to 10 cm thick rims between serpentinites and diopsidites (Fig. 3a, outcrop 1, on the map plate), are made of chlorite (60%), clinopyroxene (augite + diopside) (20%), antigorite (10-15%), ilmenite (10%), tremolite and magnetite (2-3%). Locally Ti-clinohumite occurs within these layers.

In serpentinites, boudins and layers of dark *pyroxenites* occur (Fig. 3c, d; outcrop 3 and 5, on the map plate) and are constituted by clinopyroxene (augite + diopside) (70-80%), antigorite ± chlorite (10-20%), ilmenite ± magnetite (5%), Ti-chondrodite + Ti-clinohumite (5%), tremolite (< 2%). Grain size varies from centimetre clinopyroxene porphyroclasts to the submillimetre grains of diopside, chlorite, and antigorite in the matrix. Locally (outcrop 5, on the map plate), pyroxenite layers or lenses are rimmed by Ti-chondrodite + Ti-clinohumite aggregates with minor oxides.

Yellow very fine- to coarse-grained *Olivine rich-layers* are well exposed in outcrops 2, 3, and 5 (map plate) and occur in 1 to 20 centimetres thick layers and decimetre-sized lenses. They are rich in olivine (60-90%) and contain antigorite (10-20%), magnetite ± Cr-magnetite (10%), chlorite (< 5%), Ti-chondrodite + Ti-clinohumite (< 5%), dolomite (< 2%) and diopside (< 1%).

A few millimetre-thick ochre-yellow *olivine veinlets* are composed by coarse- to fine-grained olivine (90-95%), antigorite (10-15%), and magnetite (5%). Veins show different lengths, from few centimetres to more than 1 metre and are wrapped, parallelized, and boudinaged by the dominant foliation (Fig. 2a; outcrop 1, on the map plate).

Calcite-bearing veins are undeformed, usually at a high angle with respect to the dominant foliation and constituted by calcite (90%) and minor oxides (10%).

STRUCTURAL RELATIONSHIPS

Three groups of superimposed ductile structures, indicated as pre-D₂ (comprising pre-D₂ mineral micro-aggregates and rare D₁ mesoscopic fabric elements) D₂, and D₃, and a fourth group of brittle structures affect serpentinites and the interlayered rocks. In Table 1 the main relationships between structures and rocks are schematically reported.

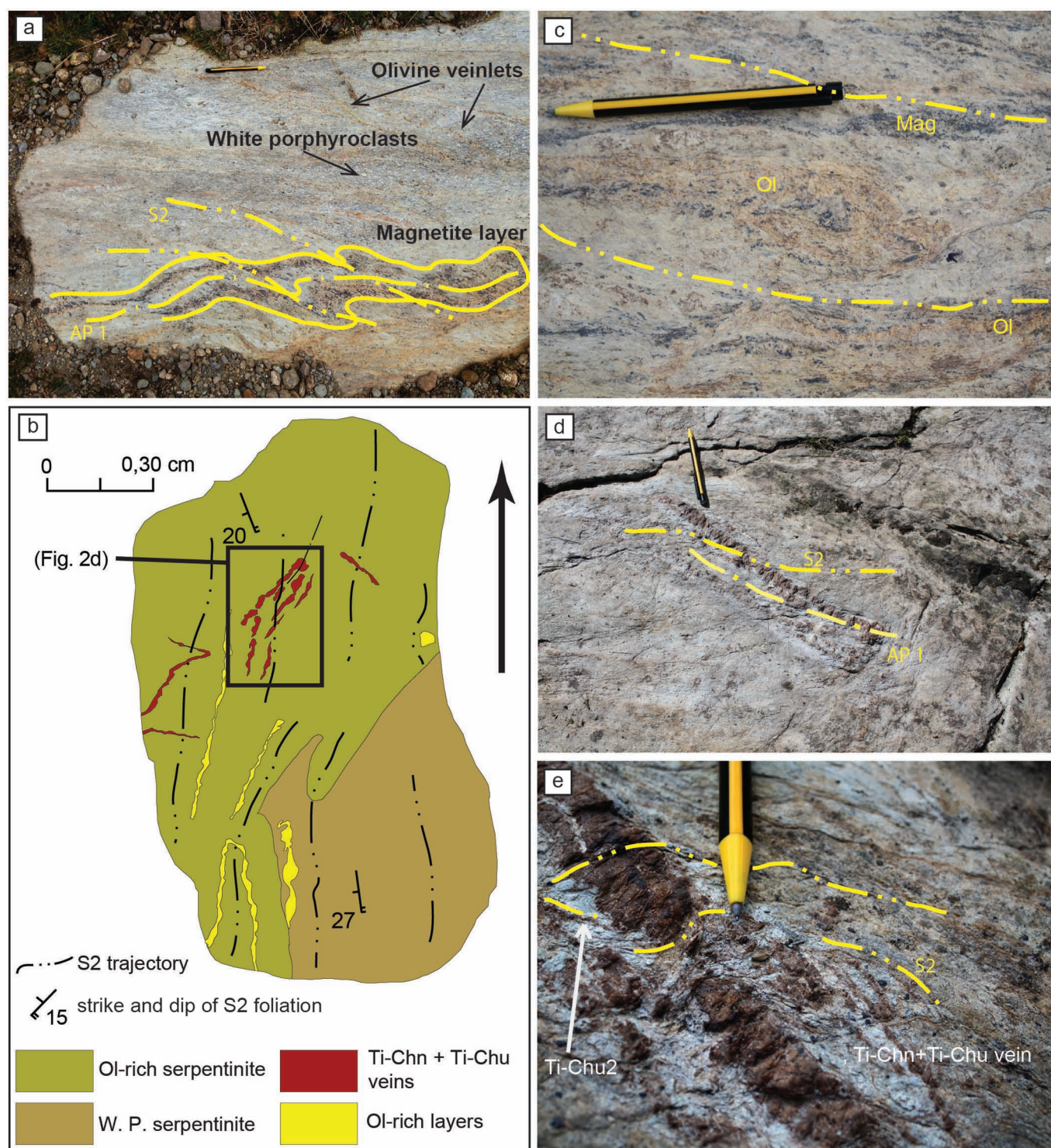


Fig. 2 - Créton area meso-structures: a) Magnetite layer in serpentinites. The magnetite layer is isoclinally folded during D_1 and crenulated and foliated during D_2 . S_2 mantles pale, lenticular porphyroclasts. In the upper part of the outcrop olivine-bearing veins are parallel to S_2 (outcrop 1); b) detail of outcrop 2a (see the map in table 1 for location): the contact between white porphyroclasts serpentinites (W.P. serpentinites) and olivine-rich serpentinites is folded by D_2 . Furthermore, Ti-chondrodite + Ti-clinohumite veins are folded by D_1 and transposed, crenulated, and foliated by D_2 ; c) relationships between S_2 and mineral layering in olivine-rich serpentinites (outcrop 1 in the map of table 1); d) Ti-chondrodite + Ti-clinohumite vein that marks a D_1 fold hinge and is transposed during D_2 (outcrop 2 in the map); this structure is included in Fig. 2b; e) Close-up on Ti-chondrodite + Ti-clinohumite lenses (Fig. 2d) intersected by S_2 with Ti-clinohumite2 in the pressure shadows.

All the rocks exposed at Créton record a dominant foliation that according to structural features, orientation, and mineral composition is identified as the same regional S_2 recognized by Rebay et al. (2012a; 2012b), Zanoni et al. (2012; 2016). Like in Valtournanche, at Créton S_2 is the structure that mostly affects the lithostratigraphic boundaries.

In places, primary mineralogical layering and boundaries between the different serpentinite types and between serpentinites and the embedded lithotypes (e.g. Fig. 3d: serpentinite - olivine-rich layers' contact) escaped the transposition during successive deformation stages. Primary foliations (S_l) corresponding to lithological boundaries between white

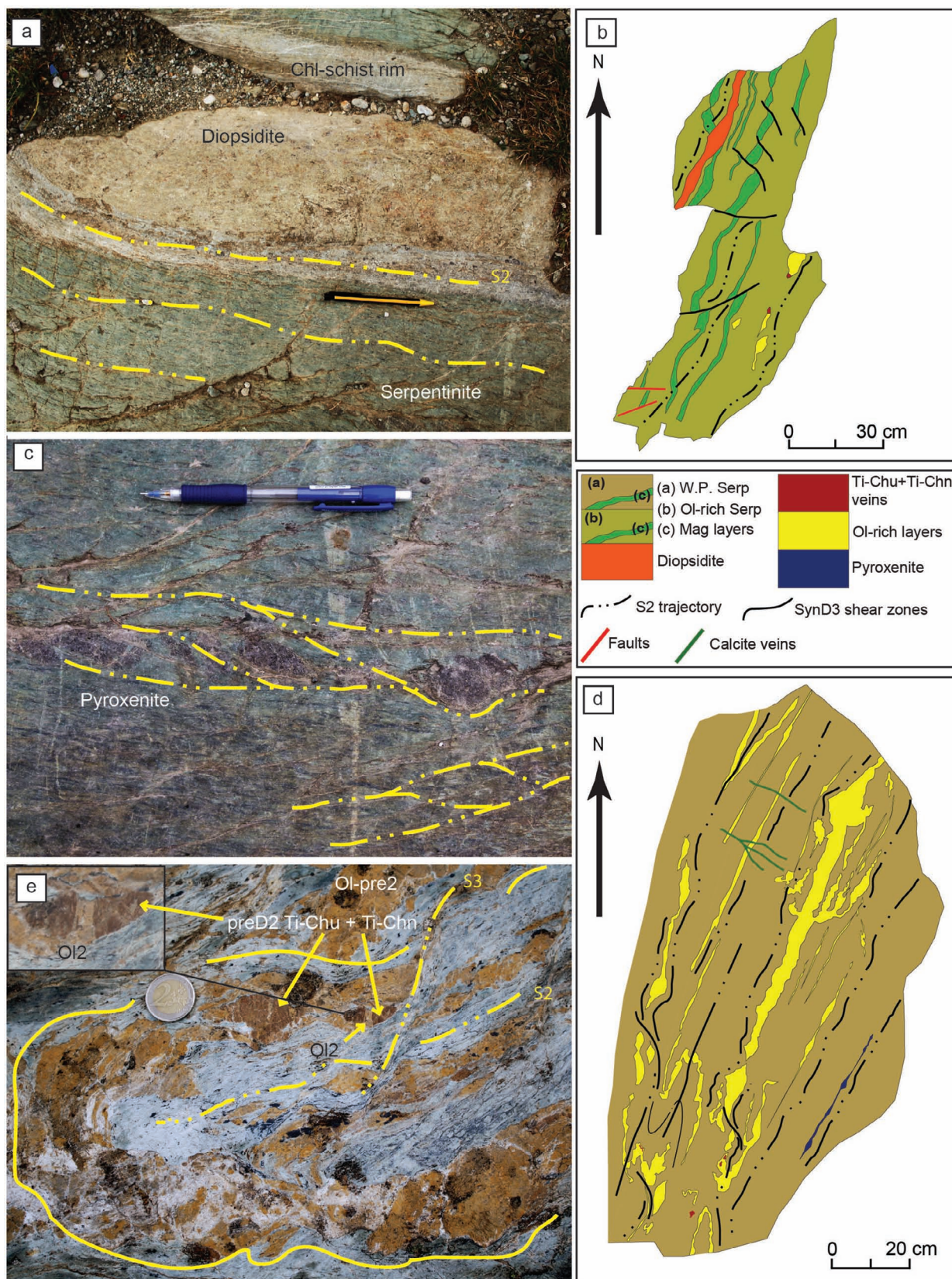


Fig. 3 - Créton area meso-structures: a) decimetre-thick layer of diopside with rims of chlorite schists parallel to S_2 (outcrop 1 in the map); b) detail of outcrop 6a: magnetite layers, olivine-rich layers and a layer of diopside, embedded in olivine-rich serpentinites, are transposed and parallelised into S_2 . A magnetite layer is crosscut by the diopside and some of the magnetite layers are crosscut by D_3 shear zones (legend between Fig. 3b and d); c) layer of aligned lenses of dark pyroxenite intersected by the composite S-C D_2 fabric (outcrop 1 in the map); d) detail map of outcrop 5, olivine-rich layers, enclosed in white porphyroclasts serpentinite (W.P. Serp.), mark D_2 fold hinges, whose flanks are folded by D_3 . S_2 is the axial plane foliation. A layer of pyroxenite is boudinaged by D_2 and parallelized into S_2 . Calcite veins crosscut S_2 foliation (legend between Fig. b and d); e) olivine-rich layer isoclinally folded and boudinaged during D_2 and intersected by S_2 foliation; the layer is displaced along a D_3 shear zone. Note the porphyroclast of pre- D_2 Ti-chondrodite + Ti-clinohumite affected by syn- D_2 boudinage with necks filled by olivine2 (outcrop 5 in the map).

porphyroclasts serpentinites and olivine-rich serpentinites are locally blurred. Where sharp, S_L is folded by or parallel to the dominant foliation.

The two types of serpentinite constitute alternating and tectonically interlayered metre-thick bands. Millimetre- to centimetre-thick and centimetre- to metre-long magnetite layers in serpentinites are strongly transposed (see for examples outcrop 1 in which all the variably sized-layers exist).

Diopside lenses and layers are parallel to the dominant foliation of serpentinites. Diopside layers locally crosscut magnetite thin layers (Fig. 3b; outcrop 6a). Also the dark pyroxenite layers (outcrops 1, 3, 5 and 6) are parallelized and boudinaged into the dominant foliation. Boudins are normally oblate. Locally, isolated centimetre-sized lenses of pyroxenites occur (outcrop 2c). Olivine-rich layers and lenses are mainly parallelized into and wrapped by the dominant foliation (outcrop 2 and 3).

Ti-chondrodite + Ti-clinohumite veins are wrapped and boudinaged within the S_2 foliation and locally veins at high angle with S_2 are variably transposed. Olivine veins are mostly parallel to S_2 (see outcrop 1) whereas Ti-chondrodite + Ti-clinohumite vein orientations are more variable with respect to the same foliation.

D_1 stage affected serpentinites, magnetite layers, olivine-rich layers, a diopside layer, and Ti-chondrodite + Ti-clinohumite veins, as shown by the D_1 fold hinges and S_1 foliation recorded in localized layers and lenses of diopside and olivine-rich layers.

In outcrop 1 (see map plate), magnetite layers are often isoclinally folded during D_1 (Fig. 2a), whereas an olivine-rich layer marks a D_1 isoclinal fold in outcrop 5. Rare S_1 foliation marked by antigorite and magnetite constitutes D_2 fold hinges in serpentinites. In outcrop 2a (see map plate), a Ti-chondrodite + Ti-clinohumite vein materializes an isoclinal D_1 fold hinge (Fig. 2d): the axial plane is sub-vertical and forms an angle of 10° with S_2 (outcrop 2a in map plate).

The olivine-rich boudinaged layers in outcrop 2b (see map plate) preserve a very rare pre- D_2 (S_1) foliation marked by layers of granoblastic olivine aggregates. In outcrop 6a, also diopside preserves a pre- D_2 (S_1) foliation, which is marked by the SPO of diopside porphyroclasts, at high angle with respect to S_2 in serpentinites.

D_2 structures consist of folds and S_2 foliation. S_2 is a mylonitic, locally composite, foliation and is the dominant fabric element in the Créton outcrops. S_2 dips W-WNW/ 14° - 65° in all the lithotypes.

D_2 folds deform the contact between the white porphyroclasts and the olivine-rich serpentinites (outcrops 1 and 2a; see map plate) with isoclinal decimetre folds associated with S_2 axial plane foliation. In both serpentinite types, S_2 is mylonitic, pervasive, and affects all the embedded lithotypes. Locally S-C foliations occur (outcrop 1, Fig. 3c), with millimetre- to centimetre-spaced C planes.

In magnetite layers, S_2 is marked by films of magnetite and antigorite. D_2 is evidenced also by an asymmetric crenulation (outcrop 1; see map plate). Generally, in these levels S_2 is marked by trails of magnetite grains (S_2 thin films). D_1 fold limbs are parallel to and intersected by S_2 (Fig. 2a). Because of its pervasiveness, S_2 obliterated S_1 axial plane foliation.

Diopside layers and lenses are parallel to S_2 that wraps also around them. The diopside layer and the associated chlorite schist rims in outcrop 1 (see map plate and Fig. 3) are pervasively foliated by S_2 , which is mylonitic in the rim.

Olivine-rich layers and lenses are enveloped by S_2 and the same layers are affected by isoclinal to open D_2 folds with centimetre to decimetre hinges (Fig. 3d, e; outcrop 5 in map plate). Syn- D_2 boudins of olivine-rich layers occur. Locally, also Ti-chondrodite + Ti-clinohumite lenses in olivine-rich layers are boudinaged during D_2 development and their necks are filled with olivine.

Dark pyroxenite layers are transposed, parallelized, and boudinaged into S_2 foliation (Fig. 3c; outcrops 3 and 5; map plate). Where S_2 is an S-C composite fabric, pyroxenite lenses are often aligned along S-planes.

Ti-chondrodite + Ti-clinohumite veins are parallelized into S_2 mineral layering of the serpentinites, and are locally boudinaged and wrapped by S_2 (outcrops 2 and 4; map plate). Veins at a high angle with S_2 are foliated and crenulated. Isolated aggregates of Ti-chondrodite + Ti-clinohumite grains are elongated into S_2 and display pressure shadows bounded by thin anastomosed layers of Ti-clinohumite (Fig. 3e) marking S_2 (outcrop 2a; map plate).

Rare D_3 centimetre-wide crenulation affects S_2 in serpentinites. D_3 fold axial surfaces dip at medium angle towards WNW and fold axes dip at a low angle towards WSW (Fig. 4a). Locally, olivine-rich layers parallel to S_2 and S_2 are deviated by syn- D_3 decimetre-long sinistral shear zones (see outcrop 5 in map plate; Fig. 3d, e).

The Créton serpentinites are finally affected by D_4 sub-vertical E-W dilatant fractures, mostly filled by calcite (outcrop 5) or by perpendicular to oblique serpentine fibres. Where fibres are oblique, fractures are actually small sinistral strike-slip faults with an offset of 5-10 cm (outcrops 1 and 6 in map plate; Fig. 4b).

MICROSTRUCTURES AND METAMORPHIC EVOLUTION

In the following, we describe the main microstructural features used to infer the mineral assemblages marking the superposed fabrics, and therefore the timing of the successive metamorphic and deformation events affecting them. Pre- D_2 relicts include D_1 structures and mineral and textural domains. D_1 structural relicts are scarce, with surfaces never exceeding one metre. Their marked re-orientation by transposition and discontinuity inhibits direct correlation of D_1 structures even in the same outcrop. Due to D_2 intense transposition, mineral relicts occurring as porphyroclasts or polygonal lenticular aggregates, wrapped by S_2 , are described as part of pre- D_2 assemblages, not being univocally relatable as D_1 fabrics as is the case for S_1 relic foliation.

In the *white porphyroclasts serpentinites*, S_2 is mylonitic, locally characterized by S-C planes and is marked by antigorite + magnetite and locally by diopside/olivine + Ti-clinohumite + chlorite. S_2 wraps millimetre-sized porphyroclasts of magnetite, olivine/clinopyroxene, Ti-clinohumite, lenses of antigorite flakes, often rimmed by a thin magnetite corona (Fig. 5a), either iso- or randomly-oriented. Locally, porphyroclasts of pre- D_2 dolomite, with dolomite rims, and apatite are enveloped by S_2 . Calcite veins occur at high angle with respect to S_2 . Occasionally, D_3 folding is associated with an incipient S_3 axial plane foliation marked by antigorite + magnetite.

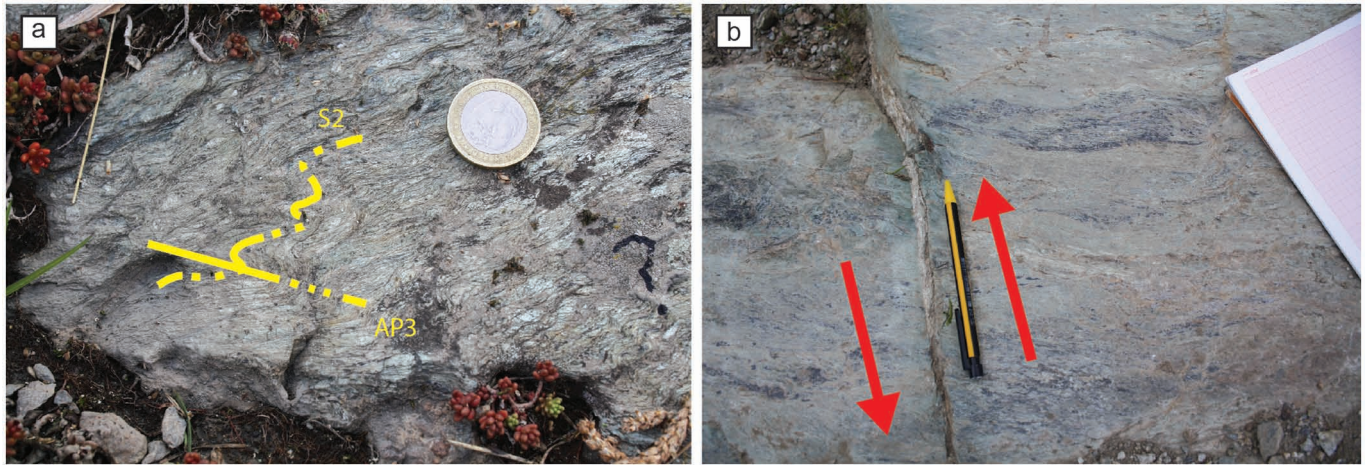


Fig. 4 - Créton area meso-structures: a) D₃ crenulation affecting S₂ foliation in serpentinites (outcrop 2 in the map); b) sinistral fault, mineralized by antigorite fibres (outcrop 6 in the map), displacing a magnetite layer.

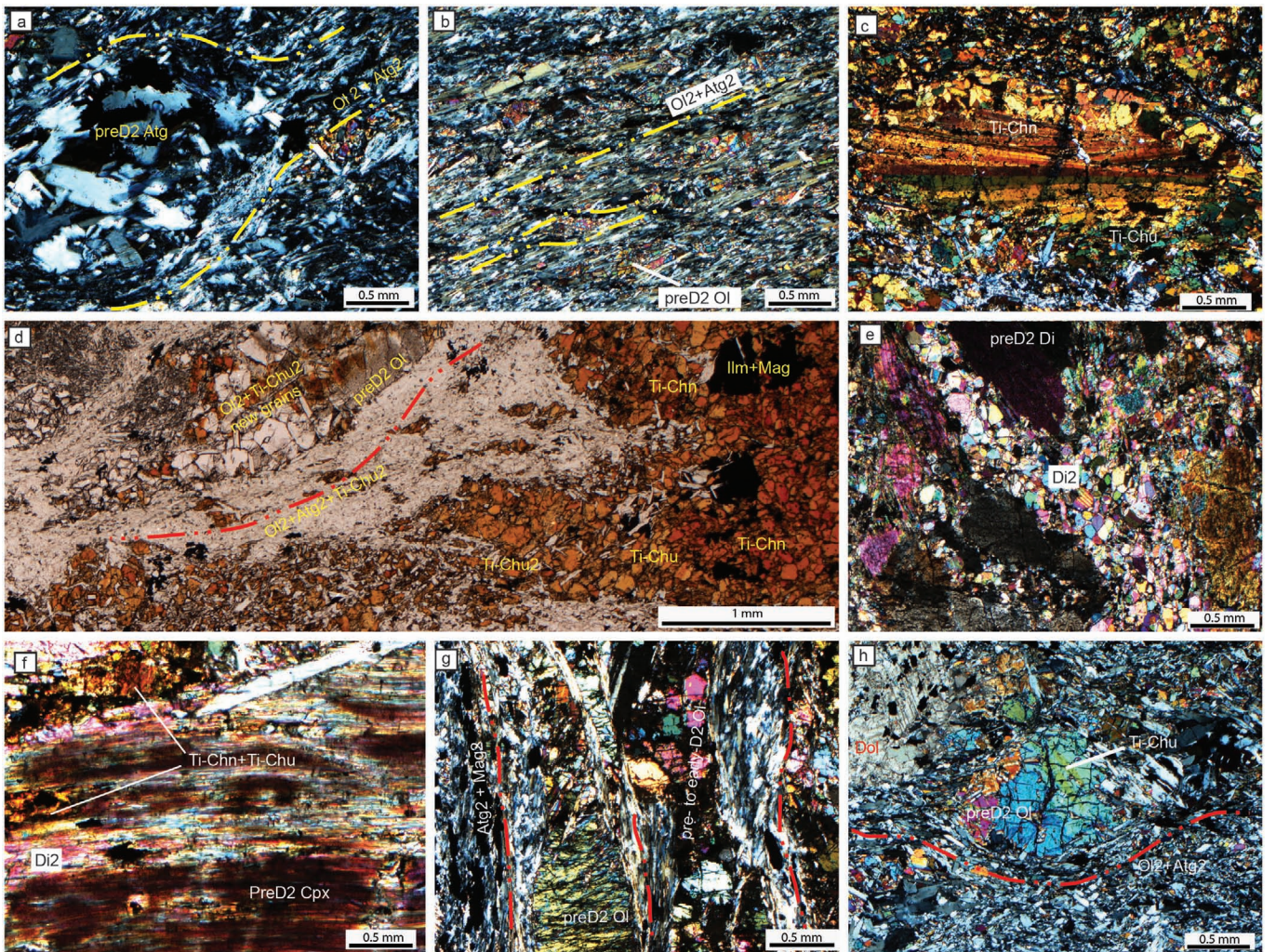


Fig. 5 - Créton area microstructures: a) completely serpentinized white lenticular domain wrapped by S₂, made of antigorite₂ and olivine₂ (crossed polars) from outcrop 1; b) olivine-rich serpentinites with S₂ marked by antigorite₂, olivine₂, and magnetite₂ from outcrop 1; S₂ wraps around pre-D₂ olivine porphyroclasts (crossed polars) partly recrystallized, as evidenced by sub-grains and new grains; c) a porphyroclast of Ti-chondrodite mantled by Ti-clinohumite (core mantle structure) from a Ti-chondrodite + Ti-clinohumite vein in outcrop 2a (crossed polars); d) pre-D₂ to early D₂ Ti-chondrodite + Ti-clinohumite + ex-spinel occupying lenticular domains and pre-D₂ olivine porphyroclasts wrapped by olivine₂ + antigorite₂ + Ti-clinohumite₂, and magnetite₂ along S₂ (outcrop 2a in map plate); e) Diopside from outcrop 1. Pre-D₂ diopside porphyroclast mantled by polygonal new grains of diopside₂; f) Ti-chondrodite + Ti-clinohumite filling fractures and cleavages of a pre-D₂ clinopyroxene porphyroclast (crossed polars; outcrop 2c); g) olivine-rich layers with S₂ at the contact with serpentinites (layers rich in antigorite, outcrop 4); S₂ wraps around porphyroclasts of pre-D₂ olivine and polygonal olivine grains and is marked by antigorite₂ and magnetite₂; crossed polars; h) olivine porphyroclast, from a boudinaged olivine veinlet, with Ti-clinohumite tapering lamellae, mantled by S₂ (from outcrop 1), crossed polars.

In the very fine-grained *olivine-rich serpentinites* olivine₂ and antigorite₂ mark the S₂ continuous and mylonitic pervasive foliation, wrapping pre-D₂ magnetite + olivine porphyroclasts (Fig. 5b). Locally, micro-layers of magnetite mark D₂ microfold hinges and scattered aggregates of Ti-clinohumite₂ occur in the matrix.

In both serpentinite types, D₃ shear zones and S₃ axial plane foliation are marked by antigorite₃ + magnetite₃ ± tremolite₃.

The millimetre-thick *magnetite layers* within the hosting serpentinites comprise pre-D₂ magnetite porphyroclasts and submillimetre grains of magnetite₂ parallel to S₂. These layers may have recorded a strong transposition during D₂ development.

The *Ti-chondrodite + Ti-clinohumite veins* preserve porphyroclasts of red-orange twinned pre-D₂ Ti-chondrodite (Fig. 5c), olivine, and spinel (currently replaced by ilmenite + magnetite) that are mantled by polygonal aggregates of Ti-chondrodite + Ti-clinohumite + ilmenite + magnetite + olivine + chlorite (related to the pre-D₂ to early D₂ stage, Luoni et al., 2018). In the veins these core-mantle structures are wrapped by S₂ underlined by Ti-clinohumite₂ + olivine₂ + antigorite₂ + magnetite₂ + chlorite₂ (Fig. 5d).

In *diopsidites* pre-D₂ diopside porphyroclasts are parallel to S₂ and often rimmed by a corona of polygonal diopside₂ (Fig. 5e). They include single grains of magnetite, antigorite, and chlorite. Porphyroclasts of pre-D₂ ilmenite, rimmed by titanite₂, and apatite also occur. S₂ is marked by diopside + antigorite + chlorite ± ilmenite. Calcite₂ is locally interstitial between diopside porphyroclasts. Randomly oriented needles of tremolite₃ and actinolite₃ overgrew S₂ foliation.

In *chlorite schists*, continuous and mylonitic S₂ foliation is marked by SPO of chlorite, diopside, and antigorite and wraps porphyroclasts of clinopyroxene, chlorite, ilmenite, and magnetite. Locally relic Ti-clinohumite grains occur. Chlorite₃ and tremolite₃ locally overgrew S₂.

In *pyroxenites* pre-D₂ clinopyroxene porphyroclasts are deformed, often kinked and rich in inclusions of antigorite, ilmenite, magnetite, chlorite, Ti-clinohumite, and Ti-chondrodite. Occasionally they preserve inclusion-free augitic cores. Some clinopyroxene porphyroclasts are extensively to completely re-crystallized in sub-grains or new grains of diopside₂ or replaced by chlorite₂. Diopside₂ inclusion-free rims also occur around some pre-D₂ clinopyroxene porphyroclasts. Locally, spinel (currently ilmenite + magnetite) occurs in aggregates within Ti-clinohumite and Ti-chondrodite polygonal aggregates. Ilmenite + magnetite + Ti-chondrodite + Ti-clinohumite polygonal aggregates rim pre-D₂ clinopyroxene and spinel (Fig. 5f). Pre-D₂ clinopyroxene is wrapped by a S₂ foliation that is marked by diopside + antigorite + Ti-clinohumite + magnetite + chlorite.

In *olivine-rich layers* (Fig. 5g), millimetre-sized porphyroclasts of pre-D₂ olivine (with magnetite, antigorite, and rare diopside inclusions) and Cr-magnetite, rimmed by magnetite₂, are mantled by sub-millimetre pre-D₂ to early D₂ polygonal aggregates of olivine + antigorite + magnetite (Luoni et al., 2018), locally with dolomite and Ti-clinohumite. Rare pre-D₂ millimetre Ti-chondrodite twinned crystals, surrounded by Ti-chondrodite + Ti-clinohumite polygonal aggregates,

have been observed. S₂ is marked by olivine + antigorite + magnetite ± Ti-clinohumite.

The *olivine veinlets* consist of rows of pre-D₂ millimetre-sized olivine porphyroclasts (Fig. 5h) that are wrapped by antigorite₂ aligned within S₂ foliation. Olivine porphyroclasts contain antigorite + magnetite inclusions, Ti-clinohumite tapering lamellae, and are rimmed by olivine₂. Towards the veins, sub-millimetre grains of olivine₂ occur in the antigorite + magnetite matrix and an olivine₂ SPO marks S₂ foliation.

In Table 2, a summary of the mineral assemblages marking the successive fabric elements is shown for each rock type.

Metamorphic evolution

The inferred parageneses, coupled with chemical analyses of selected microstructural domains (Rebay et al., 2012a; 2012b; Luoni et al., 2018), allowed constraining PT conditions under which pre-D₂, D₂ and D₃ fabrics developed. Results are synthesized in Fig. 6. Luoni et al. (2018) constrained pre-D₂ development conditions at 2.8-3.5 GPa and 600-670 °C (Ti-chondrodite + antigorite + chlorite + spinel + olivine) and the conditions for the transition from pre-D₂ to early D₂ at 2.1-3.0 GPa and 570-670 °C. Rebay et al. (2012) proposed that mineralogical foliation S₂, marked by clinopyroxene + olivine + antigorite + chlorite (± Ti-clinohumite + magnetite and ilmenite) developed at 2.2-2.8 GPa and 580-660 °C at 65 ± 5.6 Ma (Rebay et al., 2018) and successively was overprinted by the D₃ metamorphic assemblages (antigorite + tremolite) developed at 0.6-1.4 GPa and 500-600 °C. Protonoliths are dated in the same area at 165±3.2 Ma (Rebay et al., 2018). These results highlight the occurrence of an ultra-high pressure peak recorded in the ZSZ earlier than 65±5.6 Ma.

DISCUSSION

The structural observations of the Créton outcrops are summarized in a geological map showing the superposed successive Alpine structures overprinting the primary lithostratigraphic sequence.

Ti-chondrodite + Ti-clinohumite veins crosscut both magnetite layers and olivine-rich layers and lenses, while no intersection has been observed between the olivine veins and the other rocks. As the olivine veins are crosscut by S₂, they predate the transition from UHP to HP exhumation. Diopside, pyroxenite, and olivine-rich layers locally crosscut magnetite layers, indicating that magnetite layering predates their development. No structural relationships indicate a relative chronology between olivine-rich layers and pyroxenite. In particular, the locally preserved porphyroclastic texture in olivine-rich layers, with millimetre-sized olivine porphyroclasts and new grains, is similar to that described by Mercier and Nicolas (1975) in deformed lherzolite xenoliths, and could suggest that olivine-rich layers may have formed before the Alpine subduction, even if we cannot exclude that they may also be related to brucite (and serpentine) breakdown during prograde evolution. In the serpentinite outcrops adjacent to those of Créton, Rebay et al. (2018) obtained Jurassic ages (165±3.2 Ma) on zircons associated with augitic clinopyroxene derived from percolation of evolved gabbro melt, as suggested by trace element composition. These data suggest us a magmatic origin of pyroxenites in an oceanic

Table 2 - Mineral modes and assemblages marking superposed fabrics for the different rock types.

Rock type	Mineral modes	Mineral assemblages synkinematic with successive deformation stages			D3 and post D2
		pre-D2	pre-D2 to early D2	D2	
White porphyroclasts serpentinite	Atg (60-90%), Mag (10-15%), Ol/Cpx (5-10%), Cal + Dol (<5%), Locally Ti-Chu, Ilm, Chl, Ap (<5%)	Atg + Mag + Cpx/Ol + Ti-Chu + Dol + Ap	Atg + Mag + D/Ol + Ti-Chu + Chl + Cal + Dol	Atg + Mag + Chl	
Olivine-rich serpentinite	Atg (50-80%), Ol (20-30%), Mag (5-15%), Chl (<5%)	Atg + Mag + Ol + Ti-Chu	Atg + Mag + Ol + Ti-Chu	Atg + Mag + Chl	
Ti-Chn + Ti-Chu veins	Ti-Chn + Ti-Chu (70-80%), Ol (10-20%), Atg (5-10%), Mag ± Ilm (5-10%), Chl (<5%)	Ti-Chn + Ex-Spl + Ol ± Chl + Atg	Ti-Chn + Ti-Chu + Ol + Ilm + Mag + Chl + Atg	Ti-Chu + Atg + Ol + Chl + Mag	
Diopside	Di (70-80%), Atg ± Chl (10-20%), Act + Tr (5-20%), Ilm ± Trn (5%), locally Mag, Cal, and Ap (<5%)	Di + Ap + Ilm + Atg + Chl ± Mag	Di + Atg + Trn + Chl + Cal ± Ilm	Tr	
Chlorite schist	Chl (60%), Cpx (20%), Atg (10-15%), Ilm (10%), Tr, Mag (2-3%), rare Ti-Chu	Cpx + Chl + Ilm + Atg + Mag + Ti-Chu	Chl + Di + Atg + Ilm	Chl + Tr	
Pyroxenite	Cpx (70-80%), Atg ± Chl (10-20%), Ilm ± Mag (5%), Ti-Chn + Ti-Chn (5%), Tr (<2%)	Cpx (augitic core) + Spl + Atg + Chl (+ Ti-Chn)	Cpx + Atg + Chl + Ti-Chn + Ti-Chu + Ilm + Mag	Atg + Chl + Mag + Tr	
Olivine-rich layers	Ol (60-90%), Atg (10-20%), Mag ± Cr-Mag (10%), Chl (<5%), Ti-Chn + Ti-Chn (<5%), Dol (<2%), Di (<1%)	Ol + Atg + Mag + Cr-Mag + Cpx ± Ti-Chn + Chl?	Ol + Atg + Mag + Ti-Chu + Dol	Atg + Cal	

environment (Luoni et al., 2018) and allow to exclude other possible interpretations for the origin of pyroxenite layers (see Borghini et al., 2016 for a discussion). The most ancient feature at Créton is the association of white porphyroclasts serpentinite, olivine-rich serpentinite, and magnetite layers. This layering was successively affected by magmatic or metasomatic processes as testified by discordant diopsidites and olivine-rich layers.

Three phases of ductile deformation, affecting the lithostratigraphy, have been recognized at the meso-scale: D₁, D₂, and D₃, with S₂ representing the dominant foliation. Pre-D₂ relics display up to metric surfaces and consist of rootless fold hinges and lenticular crystal aggregates. S₂ is mylonitic and decimetre- to metre-sized D₂ folds are mostly isoclinal. D₃ is testified by the crenulation of S₂, rarely associated with a differentiated axial plan S₃ foliation. During the last brittle D₄ stage serpentine or calcite filled fracture sets, locally display a centimetre-scale dislocation.

The kinematic, orientation and style compatibility, coupled with the marking assemblages, allow the correlation of D₂ Créton stage with the D₂ syn-high pressure stage proposed for the adjacent serpentinites, which is dated at 65±5.6 Ma (Rebay et al., 2012a; 2012b; 2018). PT conditions inferred for D₂ development suggest a T/depth ratio of 7-11 °Ckm⁻¹. The ultra-high pressure assemblage marking pre-D₂ fabric (Ti-chondrodite + antigorite + chlorite + spinel + olivine for estimated T of 600-670 °C and P of 2.8-3.5 GPa after Luoni et al., 2018) indicate a T/depth ratio of 6-8 °Ckm⁻¹. Also D₃ structures can be related to the D₃ described by Rebay et al. (2012a; 2012b), contemporaneous to amphibole-epidote facies conditions; here physical conditions of metamorphism during D₃ indicate a T/depth ratio comprised between 21 and 26 °Ckm⁻¹. D₄ developed at shallow structural level at the end of the exhumation history. Moreover, structural and metamorphic evolution and radiometric ages obtained for D₂ development indicate that ultra-high pressure conditions were reached before at least 60 Ma. As shown in Fig. 6, pre-D₂ and D₂ conditions are close to those of cold subduction zones (Cloos, 1993), with a P-climax characterized by a considerably lower thermal state with respect to the earlier stages of ZSZ serpentinite exhumation (D₂). Latest stages of decompression occurred under higher temperatures, close to the intraplate normal thermal state (Cloos, 1993), compatible with continental collision.

The detection of ultra-high pressure rocks at Créton individuates another UHP unit that must be added to that of Cignana Lake Unit (Reinecke, 1991; Groppo et al., 2009; Frezzotti et al., 2011). Both these oceanic lithosphere crustal slices occur close to the tectonic contact between CZ and ZSZ. Since UHP Ti-Chn-bearing assemblages in serpentinites, have been exclusively detected in upper Valtouranche (Créton and Cignana: Luoni et al., 2018; Gilio et al., 2019), they are not sufficient to infer UHP conditions to the serpentinites of the whole ZSZ. Indeed, the detection of UHP rocks at Créton individualizes another UHP unit that must be added to that of Cignana Lake Unit, already identified on the basis of coesite- and diamond-bearing assemblages in oceanic metasediments (Reinecke, 1991; Groppo et al., 2009; Frezzotti et al., 2011). Both these oceanic slices occur close to the tectonic contact between CZ and ZSZ. In addition, the heterogeneous and diachronic tectono-metamorphic evolutions recorded in different portions of the ZSZ (see Rebay et al., 2018 and references therein) suggest that this domain can be considered a tectono-metamorphic puzzle rather than a homogeneous subducted and exhumed coherent slab.

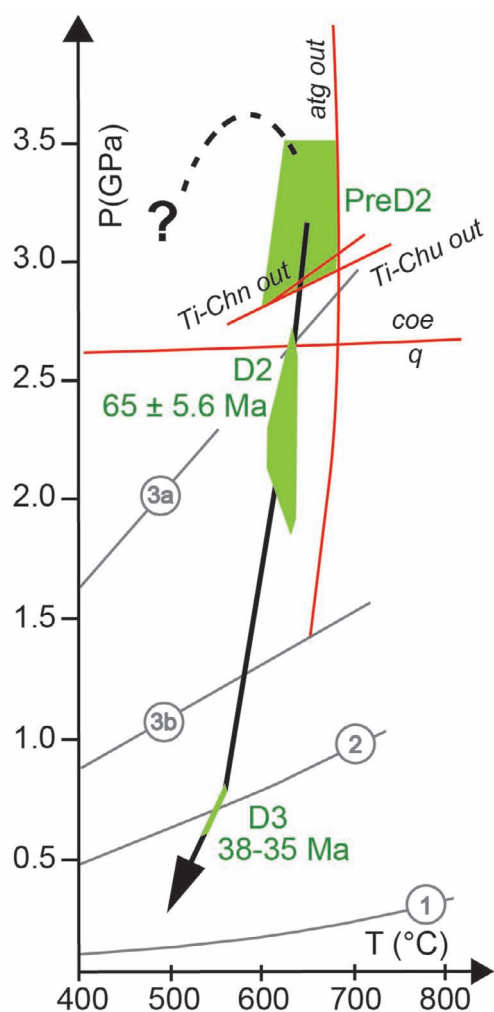


Fig. 6 - P-T-d-t evolution of the Valtournanche serpentinites integrating the physical conditions of metamorphism as estimated by Rebay et al. (2012) and Luoni et al. (2018) and age data from Rebay et al. (2018). Ti-chondrodite out, Ti-clinohumite out, antigorite out curves are from Shen et al. (2015) (modified after Luoni et al., 2018). Grey geotherms are after Cloos et al. (1993): (1) near spreading ridge or volcanic arc; (2) normal gradient of old plate interior; (3a) cold subduction zones; (3b) warm subduction zones.

CONCLUSION

In conclusion, the type of multiscale structural analyses (from 1:200 to 1:20 to microscale) here used may open possibilities of describing and deciphering more complex evolutions in apparently monotonous rocks such as serpentinites, which are usually considered to display weak variations in mineral assemblages.

Créton serpentinites represent a heterogeneous oceanic peridotite slice with magnetite layers, in which layers and lenses of scarcely preserved pyroxenites and olivine-rich layers, and completely re-equilibrated diopsidites are embedded. These rocks reached and heterogeneously recorded ultra-high pressure peak conditions, testified by Ti-chondrodite and Ti-clinohumite bearing pre-D₂ assemblages (Shen et al., 2015; González-Jiménez et al., 2017; Luoni et al., 2018) under highly depressed thermal regime before Palaeocene, and were exhumed up to D₂ PT conditions (Rebay et al., 2012a; 2012b) still in a depressed thermal state, typical of cold subduction

zones. On the contrary, the last stages of exhumation (D₃-D₄) occurred under considerably higher thermal state suggesting the contemporaneity with the Alpine continental collision.

ACKNOWLEDGEMENTS

Insightful reviews by Vicente López Sánchez-Vizcaíno and Marco Scambelluri greatly improved the first version of the manuscript and are acknowledged. G. Gosso gave useful advice during field-work and C. Malinverno made the thin sections. PL thanks Paolo Papone and Ugo Zuretti for their kind hospitality during field work. PL is grateful to Studio Ciocca. Funding by University of Milano PSR2018_DZANONI “Analisi strutturale delle catene collisionali”. Results here presented have been developed in the frame of the MIUR Project “Dipartimenti di Eccellenza 2017-Le geoscienze per la società: risorse e loro evoluzione (Work-package 3, Tasks 3.3-3.4)”. The supplementary material is available at the web address www.ofioliti.it

REFERENCES

- Angiboust S., Agard P., Jolivet L. and Beyssac O., 2009. The Zermatt-Saas ophiolite: The largest (60-km wide) and deepest (c. 70-80 km) continuous slice of oceanic lithosphere detached from a subduction zone? *Terra Nova*, 21: 171-180. doi: 10.1111/j.1365-3121.2009.00870
- Baletti L., Zanoni D., Spalla M.I. and Gosso G., 2012. Structural and petrographic map of the Sassa gabbro complex (Dent Blanche nappe, Austroalpine tectonic system, Western Alps, Italy). *J. Maps*, 8 (4): 413-430. doi: 10.1080/17445647.2012.745678
- Ballèvre M. and Merle O., 1993. The Combin Fault: compressional reactivation of a Late Cretaceous-Early Tertiary detachment fault in the Western Alps. *Schweiz. Miner. Petrol. Mitt.*, 73 (2): 205-227.
- Barnicoat A.C. and Fry N., 1986. High-pressure metamorphism of the Zermatt-Saas ophiolite, Switzerland. *J. Geol. Soc.*, 143 (4): 607-618.
- Beauregard P., 1967. Die Ophiolite der Zone von Zermatt-Saas Fee. *Beitr. Geol. Karte Schweiz*, 132: 1-130.
- Bigi G., Castellarin A., Coli M., Dal Piaz G.V., Sartori R., Scandone P. and Vai G.B., 1990. Structural Model of Italy, sheets 1-2, In: C.N.R., P.F.G. (Ed.). S.E.L.C.A., Florence.
- Borghini G., Rampone E., Zanetti A., Class C., Cipriani A., Hofmann A.W., and Goldstein S.L., 2016. Pyroxenite layers in the Northern Apennines upper mantle (Italy) - generation by pyroxenite melting and melt infiltration. *J. Petrol.*, 57 (4): 625-653.
- Boudier F. and Nicolas A., 1985. Harzburgite and lherzolite subtypes in ophiolitic and oceanic environments. *Earth Planet. Sci. Lett.*, 76 (1-2): 84-92.
- Bowtell S.A., Cliff R.A. and Barnicoat A.C., 1994. Sm-Nd isotopic evidence on the age of eclogitization in the Zermatt-Saas ophiolite. *J. Metam. Geol.*, 12 (2): 187-196. doi: 10.1111/j.1525-1314.1994.tb00013.x.
- Bucher K. and Grapes R., 2009. The eclogite-facies Allalin gabbro of the Zermatt-Saas ophiolite, Western Alps: A record of subduction zone hydration. *J. Petrol.*, 50 (8): 1405-1442. doi: 10.1093/petrology/egp035
- Bucher K., Fazis Y., De Capitani C. and Grapes R., 2005. Blueschists, eclogites, and decompression assemblages of the Zermatt-Saas ophiolite: High-pressure metamorphism of subducted Tethys lithosphere. *Am. Miner.*, 90 (5-6): 821-835. doi: 10.2138/am.2005.1718
- Cartwright I. and Barnicoat A.C., 2002. Petrology, geochronology, and tectonics of shear zones in the Zermatt-Saas and Combin zones of the Western Alps. *J. Metam. Geol.*, 20 (2): 263-281.

- Cloos M., 1993. Lithospheric buoyancy and collisional orogenesis - Subduction of oceanic plateaus, continental margins, island arcs, spreading ridges, and seamounts. *Geol. Soc. Am. Bull.*, 105: 715-737.
- Connors K.A. and Lister G.S., 1995. Polyphase deformation in the western Mount Isa Inlier, Australia: episodic or continuous deformation? *J. Struct. Geol.*, 17 (3): 305-328. doi: 10.1016/0191-8141(94)00057-7
- Dal Piaz G.V., 1974. Le métamorphisme de haute pression et basse température dans l'évolution structurale du bassin ophiolitique alpine-apenninique. *Schweiz. Miner. Petrogr. Mitt.*, 54 (2/3): 399-424.
- Dal Piaz G.V., 1988. Revised setting of the Piedmont Zone in the northern Aosta Valley, Western Alps. *Ofioliti*, 13: 157-162.
- Dal Piaz G.V., 1992. Guide geologiche regionali. Vol. 3/1: Le Alpi dal Monte Bianco al Lago Maggiore. *Soc. Geol. It., BeMa*, Roma-Milano.
- Dal Piaz G.V., 1999. The Austroalpine-Piedmont nappe stack and the puzzle of Alpine Tethys. 3rd Workshop on Alpine geological studies. *Mem. Sci. Geol.*: 155-176.
- Dal Piaz G.V. and Ernst W.G., 1978. Areal geology and petrology of eclogites and associated metabasites of the Piemonte ophiolite nappe, Breuil-St. Jacques area, Italian Western Alps. *Tectonophysics*, 51: 99-126.
- Dal Piaz G.V., Cortiana G., Del Moro A., Martin S., Pennacchioni G. and Tartarotti P., 2001. Tertiary age and paleostructural inferences of the eclogitic imprint in the Austroalpine outliers and Zermatt-Saas ophiolite, western Alps. *Int. J. Earth Sci.*, 90: 668-684. doi: 10.1007/s005310000177
- Dal Piaz G.V., Lombardo B. and Gosso G., 1983. Metamorphic evolution of the Mt. Emilius klippe, Dent Blanche nappe, western Alps. *Am. J. Sci.*, 283A: 438-458.
- Dale C.W., Burton K.W., Pearson D.G., Gannoun A., Alard O., Argles T.W. and Parkinson I.J., 2009. Highly siderophile element behaviour accompanying subduction of oceanic crust: Whole rock an (5):1394-1416. doi: 10.1016/j.gca.2008.11.036
- Ernst W.G. and Dal Piaz G.V., 1978. Mineral parageneses of eclogitic rocks and related mafic schists of the Piemonte ophiolite nappe, Breuil-St. Jacques area, Italian Western Alps. *Am. Mineral.*, 63 (7-8): 621-640.
- Forster M., Lister G., Compagnoni R., Giles D., Hills Q., Betts P. and Tamagno E., 2004. Mapping of oceanic crust with "HP" to "UHP" metamorphism: The Lago di Cignana Unit, (Western Alps)'. In: G. Pasquarè, C. Venturini and G. Gropelli (Eds.), *Mapping geology in Italy, Map 33 S.EL.CA.*, Firenze, p. 279-286.
- Frezzotti M.L., Selverstone J., Sharp Z.D. and Compagnoni R., 2011. Carbonate dissolution during subduction revealed by diamond-bearing rocks from the Alps. *Nat. Geosci.*, 4 (10): 703-706. doi: 10.1038/ngeo1246.
- De Giusti F., Dal Piaz G.V., Massironi M. and Schiavo A., 2003. Carta geotettonica della Valle d'Aosta. *Mem. Sci. Geol.*, 55: 129-149.
- Gilio M., Scambelluri M., Agostini S., Godard M., Peters D., and Pettke T., 2019. Petrology and geochemistry of serpentinites associated with the ultra-high pressure Lago di Cignana Unit (Italian Western Alps). *J. Petrol.* doi: 10.1093/petrology/egz030
- González-Jiménez J.M., Plissart G., Garrido L.N., Padrón-Navarta J.A., Aiglsperger T., Romero R., Reich M., Barra F. and Morata D., 2017. Ti-clinohumite and Ti-chondrodite in antigorite serpentinites from Central Chile: evidence for deep and cold subduction. *Eur. Mineral.*, 29 (6): 959-970. doi: 10.1127/ejm/2017/0029-2668
- Gosso G. and Spalla M.I., 2009. Stratigraphy in the continental crust: lithologic and tectonic records. *Ital. J. Geosci.*, 128 (2): 473-482.
- Gosso G., Brizio D., Deregis C., Eusebio A., Gallo M., Rattalino E., Rossi F. and Toso F., 1983. Due cinematiche possibili per la coppia di falde Brianzonese ligure-Flysch ad Elmintoidi, *Mem. Soc. Geol. It.*, 26 (2): 463-472.
- Gosso G., Messiga B., Rebay G., and Spalla M.I., 2010. Interplay between deformation and metamorphism during eclogitization of amphibolites in the Sesia-Lanzo Zone of the Western Alps. *Int. Geol. Rev.*, 52 (10-12): 1193-1219.
- Gosso G., Rebay G., Roda M., Spalla M.I., Tarallo M., Zanoni D. and Zucali M., 2015. Taking advantage of petrostructural heterogeneities in subduction-collisional orogens, and effect on the scale of analysis. *Per. Miner.*, 84: 779-825.
- Grigull S., Krohe A., Moos C., Wassmann S. and Stöckhert B., 2012. "Order from chaos": A field-based estimate on bulk rheology of tectonic mélanges formed in subduction zones. *Tectonophysics*, 568-569: 86-101. doi: 10.1016/j.tecto.2011.11.004
- Groppo C., Beltrando M. and Compagnoni R., 2009. The P-T path of the ultra-high pressure Lago Di Cignana and adjoining high-pressure meta-ophiolitic units: Insights into the evolution of the subducting Tethyan slab. *J. Metam. Geol.*, 27 (3): 207-231. doi: 10.1111/j.1525-1314.2009.00814
- Hobbs B.E., Means W.D. and Williams P.F., 1976. An outline of structural geology. Wiley, New York, 571 pp.
- Johnson S.E. and Duncan A.C., 1992. Fault identification in complexly deformed schist terrains: examples from the USA and Australia. *Tectonophysics*, 216 (3-4): 291-308.
- Kienast J.R., 1983. Le métamorphisme de haute pression et basse température (éclogites et schistes bleus): données nouvelles sur la pétrologie des roches de la croûte océanique subduite et des sédiments associés VI. *Univ. Pierre et Marie Curie*, 389 pp.
- van der Klauw S.N.G.C., Reinecke T. and Stöckhert B., 1997. Exhumation of ultrahigh-pressure metamorphic oceanic crust from Lago di Cignana, Piemontese zone, western Alps: the structural record in metabasites. *Lithos*, 41 (1-3): 79-102. doi: 10.1016/S0024-4937(97)82006-3
- Li X.P., Rahn M. and Bucher K., 2004. Serpentinites of the Zermatt-Saas ophiolite complex and their texture evolution. *J. Metam. Geol.*, 22 (3): 159-177. doi: 10.1111/j.1525-1314.2004.00503.x
- Luoni P., Rebay G., Spalla M.I. and Zanoni D., 2018. UHP Ti-chondrodite in the Zermatt-Saas serpentinite: Constraints on a new tectonic scenario. *Am. Mineral.*, 103 (6): 1002-1005. doi: http://doi.org/10.2138/am-2018-6460
- Martin S., Tartarotti P. and Dal Piaz G.V., 1994. Alpine ophiolites: a review. *Bull. Geofis. Teor. Appl.*, 36: 175-219.
- Mercier J.C., and Nicolas A., 1975. Textures and fabrics of upper-mantle peridotites as illustrated by xenoliths from basalts. *J. Petrol.*, 16 (1): 454-487.
- de Meyer C.M., Baumgartner L.P., Beard B.L. and Johnson C.M., 2014. Rb-Sr ages from phengite inclusions in garnets from high pressure rocks of the Swiss Western Alps. *Earth Planet. Sci. Lett.*, 395: 205-216. doi: 10.1016/j.epsl.2014.03.050
- Meyer J., 1983. *Mineralogie und petrologie des Allalin gabbros*. Univ. Basel.
- Nicolas A. and Boudier F., 2003. Where ophiolites come from and what they tell us. In: Y. Dilek and S. Newcomb (Eds.), *Ophiolite concept and the evolution of geological thought*. *Geol. Soc. Am. Soc.*, 373: 137-152.
- Passchier C.W., 1990. *Field geology of high-grade gneiss terrains*. Springer V., New York, 147 pp.
- Pleuger J., Roller S., Walter J.M., Jansen E. and Froitzheim N., 2007. Structural evolution of the contact between two Penninic nappes (Zermatt-Saas zone and Combin zone, Western Alps) and implications for the exhumation mechanism and paleogeography. *Int. J. Earth Sci.*, 96 (2): 229-252. doi: 10.1007/s00531-006-0106-6
- Polino R., Dal Piaz G.V. and Gosso G., 1990. Tectonic erosion at the Adria margin and accretionary processes for the Cretaceous orogeny of the Alps. *Mém. Soc. Géol. Fr.*, 156 (6): 345-367.
- Rebay G., Spalla M.I. and Zanoni D., 2012a. Interaction of deformation and metamorphism during subduction and exhumation of hydrated oceanic mantle: Insights from the Western Alps. *J. Metam. Geol.*, 30 (7): 687-702. doi: 10.1111/j.1525-1314.2012.00990.x
- Rebay G., Spalla M.I. and Zanoni D., 2012b. Multi-scale structural analysis of the serpentinites of the upper Valtouranche. *Rend. online Soc. Geol. It.*, 22: 197-200.
- Rebay G., Zanoni D., Langone A., Luoni P., Tiepolo M. and Spalla M.I., 2018. Dating of ultramafic rocks from the Western Alps ophiolites discloses Late Cretaceous subduction ages in the Zermatt-Saas Zone. *Geol. Mag.*, 155 (2): 298-315. doi: 10.1017/S0016756817000334

- Reinecke T., 1991. Very high pressure metamorphism and uplift of coesite-bearing metasediments from the Zermatt-Saas Zone, Western Alps. *Eur. J. Miner.*, 3: 7-17.
- Reinecke T., 1998. Prograde high- to ultrahigh-pressure metamorphism and exhumation of oceanic sediments at Lago di Cignana, Zermatt-Saas Zone, western Alps. *Lithos*, 42 (3-4): 147-189. doi: 10.1016/S0024-4937(97)00041-8
- Ring U., 1995. Horizontal contraction or horizontal extension? Heterogeneous Late Eocene and Early Oligocene general shearing during blueschist and greenschist facies metamorphism at the Pennine-Austroalpine boundary zone in the Western Alps. *Geol. Rundsch.*, 84 (4): 843-859.
- Rubatto D., Gebauer D. and Fanning M., 1998. Jurassic formation and Eocene subduction of the Zermatt-Saas-Fee ophiolites: implications for the geodynamic evolution of the Central and Western Alps. *Contrib. Miner. Petr.*, 132: 269-287.
- Scambelluri M., Müntener O., Hermann J., Piccardo G.B. and Trommsdorff V., 1995. Subduction of water into the mantle: History of an Alpine peridotite. *Geology*, 23 (5): 459-462.
- Shen T., Hermann J., Zhang L., Lü Z., Padrón-Navarta J.A., Xia B. and Bader T., 2015. UHP metamorphism documented in Ti-chondrodite- and Ti-clinohumite-bearing serpentinized ultramafic rocks from Chinese South-western Tianshan. *J. Petrol.*, 56 (7): 1425-1458. doi: 10.1093/petrology/egv042
- Skora S., Lapen T.J., Baumgartner L.P., Johnson C.M., Hellebrand E. and Mahlen N.J., 2009. The duration of prograde garnet crystallization in the UHP eclogites at Lago di Cignana, Italy. *Earth Planet. Sci. Lett.*, 287: 402-411.
- Skora S., Mahlen N.J., Johnson C.M., Baumgartner L.P., Lapen T.J., Beard B.L. and Szilvagy E.T., 2015. Evidence for protracted prograde metamorphism followed by rapid exhumation of the Zermatt-Saas Fee ophiolite. *J. Metam. Geol.*, 33 (7): 711-734. doi: 10.1111/jmg.12148
- Spalla M.I. and Zucali M., 2004. Deformation vs. metamorphic re-equilibration heterogeneities in polymetamorphic rocks: a key to infer quality P-T-d-t path. *Per. Mineral.*, 73: 249-257.
- Spalla M.I., Zucali M., Di Paola S. and Gosso G., 2005. A critical assessment of the tectono-thermal memory of rocks and definition of tectono-metamorphic units: evidence from fabric and degree of metamorphic transformations. *J. Geol. Soc. London Spec. Publ.*, 243 (1): 227-247.
- Springer K., Lapen T.J., Baumgartner L.P., Johnson C.M. and Beard B.L., 2009. Sm-Nd geochronology of the Zermatt-Saas ophiolite, northern Italy. *Geochim. Cosmochim. Acta, Suppl.*, 73: A1258.
- Tartarotti P., Festa A., Benciolini L. and Balestro G., 2017. Record of Jurassic mass transport processes through the orogenic cycle: Understanding chaotic rock units in the high-pressure Zermatt-Saas ophiolite (Western Alps). *Lithosphere-U.S.*, 9 (3): 399-407. doi: 10.1130/L605.1
- Weber S. and Bucher K., 2015. An eclogite-bearing continental tectonic slice in the Zermatt-Saas high-pressure ophiolites at Trockener Steg (Zermatt, Swiss Western Alps). *Lithos*, 232: 336-359. doi: 10.1016/j.lithos.2015.07.010
- Weber S., Sandmann S., Miladinova I., Fonseca R.O., Froitzheim N., Munker C. and Bucher K., 2015. Dating the initiation of Piemonte-Liguria Ocean subduction: Lu-Hf garnet chronometry of eclogites from the Theodul Glacier Unit (Zermatt-Saas zone, Switzerland). *Swiss J. Geosci.*, 108 (2): 183-199. doi: 10.1007/s00015-015-0180-5
- Whitney D.L. and Evans B.W., 2010. Abbreviations for names of rock-forming minerals. *Am. Miner.*, 95: 185-187. doi: 10.2138/am.2010.3371
- Zanoni D., Rebay G., Bernardoni J. and Spalla M.I., 2012. Using multiscale structural analysis to infer high-/ultrahigh-pressure assemblages in subducted rodingites of the Zermatt-Saas Zone at Valtournanche, Italy. *J. Virt. Expl.*, 41: 2-30. doi: 10.3809/jvirtex.2011.00290
- Zanoni D., Rebay G. and Spalla M.I., 2016. Ocean floor and subduction record in the Zermatt-Saas rodingites, Valtournanche, Western Alps. *J. Metam. Geol.*, 34: 941-961. doi: 10.1111/jmg.12215
- Zingg A., Handy M.R., Hunziker J.C. and Schmid S.M., 1990. Tectonometamorphic history of the Ivrea Zone and its relationship to the crustal evolution of the Southern Alps. *Tectonophysics*, 182 (139): 169-192.
- Zucali M., Spalla M.I. and Gosso G., 2002. Fabric evolution and reaction rate as correlation tool: the example of the Eclogitic Micaschists Complex in the Sesia-Lanzo Zone (Monte Mucrone - Monte Mars, Western Alps Italy). *Schweiz. Miner. Petr. Mitt.*, 82: 429-454.

Received, January 9, 2019
Accepted, June 18, 2019

